

# Optimization of Secondary Air Injection in a Wood-Burning Cookstove: an Experimental Study

*Julien J. Caubel<sup>†‡\*</sup>, Vi H. Rapp<sup>‡</sup>, Sharon S. Chen<sup>‡</sup>, Ashok J. Gadgil<sup>‡¶</sup>*

<sup>†</sup> Department of Mechanical Engineering, University of California, Berkeley, Berkeley, California 94720, United States

<sup>‡</sup> Environmental Technologies Area, Lawrence Berkeley National Laboratory, Berkeley, California 94720, United States

<sup>¶</sup> Department of Civil and Environmental Engineering, University of California, Berkeley, Berkeley, California 94720, United States

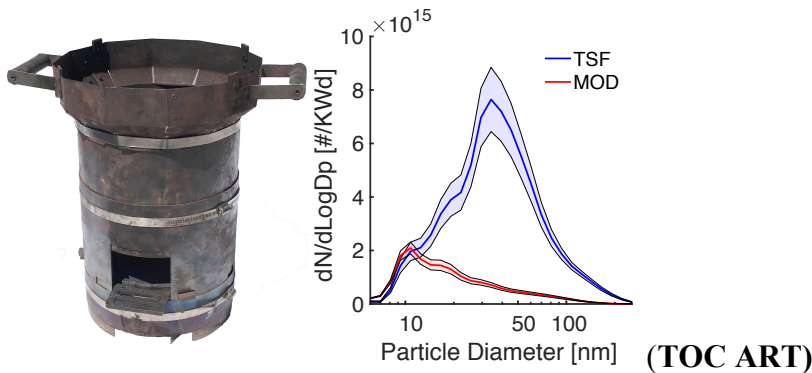
\*1 Cyclotron Road MS 90R2121, Berkeley, CA 94720

Phone: 01-646-596-3845; E-mail: [jcaubel@lbl.gov](mailto:jcaubel@lbl.gov)

Published in Environmental Science and Technology, **2018**, 52 (7), pp 4449–4456

DOI: 10.1021/acs.est.7b05277

1 **ABSTRACT**



5 **Nearly 40% of the world’s population regularly cooks on inefficient biomass stoves**  
6 **that emit harmful airborne pollutants, such as particulate matter (PM).** Secondary air  
7 injection can significantly reduce PM mass emissions to mitigate the health and climate impacts  
8 associated with biomass cookstoves. However, secondary air injection can also increase the  
9 number of ultrafine particles emitted, which may be more harmful to health. This research  
10 investigates the effect of secondary air injection on the mass and size distribution of PM emitted  
11 during solid biomass combustion. An experimental biomass cookstove platform and parametric  
12 testing approach are presented to identify and optimize critical secondary air injection parameters  
13 that reduce PM and other pollutants. Size-resolved measurements of PM emissions were  
14 collected and analyzed as a function of parametric stove design settings. The results show that  
15 PM emissions are highly sensitive to secondary air injection flow rate and velocity. Although  
16 increasing turbulent mixing (through increased velocity) can promote more complete  
17 combustion, increasing the total flow rate of secondary air may cause localized flame quenching  
18 that increases particle emissions. Therefore, biomass cookstoves that implement secondary air  
19 injection should be carefully optimized and validated to ensure that PM emission reductions are  
achieved throughout the particle size range.

## 20 INTRODUCTION

21 Nearly 40% of the world's population relies on biomass stoves for their daily cooking  
22 needs.<sup>1</sup> These stoves are often three stones supporting a cooking pot above a burning bed of solid  
23 biomass, known as a three stone fire (TSF). These rudimentary stoves are significant sources of  
24 harmful airborne pollutants, such carbon monoxide (CO) and particulate matter (PM).<sup>2</sup> Exposure  
25 to indoor air pollution from solid biomass combustion is the world's greatest environmental  
26 health risk, causing nearly 4 million premature deaths annually.<sup>3</sup> Many clean and efficient  
27 biomass stoves have been designed to reduce exposure to these harmful emissions. Since wood is  
28 a common primary cooking fuel, many improved cookstoves are natural draft, wood-burning  
29 designs that provide around 50% mass emission reductions relative to a TSF (when normalized  
30 by cooking power).<sup>4-6</sup> The World Health Organization (WHO) recommends that 24-hour average  
31 PM concentrations remain below 25  $\mu\text{g}/\text{m}^3$ .<sup>7</sup> However, a TSF can generate average indoor  
32 concentrations exceeding 1000  $\mu\text{g}/\text{m}^3$ , and many natural draft, wood-burning cookstoves do not  
33 adequately reduce emissions to meet WHO guidelines and significantly alleviate health  
34 impacts.<sup>8,9</sup>

35 Since harmful emissions from biomass stoves are generated by incomplete fuel oxidation,  
36 emission reduction strategies generally rely on improvements in the combustion process.  
37 Complete fuel oxidation requires an adequate supply of oxygen in the combustion zone, and  
38 benefits from: (1) Combustion temperatures above  $\sim 850^\circ\text{C}$ , (2) Sufficient residence time for the  
39 gas-phase fuel in the combustion zone, and (3) Turbulence to promote mixing of gas-phase fuel  
40 and oxygen.<sup>10</sup> In natural draft cookstoves, combustion of the gas-phase fuel is a buoyancy- and  
41 diffusion-driven process that generates little turbulence, leading to fuel-rich combustion zones  
42 where oxidation is incomplete. Although natural draft cookstoves designed to consume improved

43 biomass fuels (such as pellets) can reduce harmful emissions, the additional fuel processing cost  
44 and lack of distribution infrastructure limit adoption in the poor, remote communities most at  
45 risk.<sup>6,11</sup>

46 In many applications of solid fuel combustion, such as boilers, heaters, and cookstoves,  
47 an effective method for reducing unwanted emissions is injecting secondary air into the  
48 combustion chamber.<sup>12-17</sup> Carefully positioned, high-velocity jets of secondary air generate  
49 turbulent mixing that is typically lacking in naturally drafted, diffusion flames. Air injection also  
50 provides oxygen directly to fuel-rich zones, thereby promoting more complete oxidation and  
51 higher combustion temperatures.<sup>12,18,19</sup> However, non-preheated secondary air is much cooler  
52 than the combustion gases, and when improperly injected, can lead to lower combustion  
53 temperatures that result in incomplete fuel oxidation and more pollutant emissions.<sup>20</sup>  
54 Furthermore, researchers have shown that secondary air injection can reduce the mass of PM  
55 emitted during cooking, but may increase the number of ultrafine particles generated.<sup>21</sup>  
56 Inhalation of these ultrafine particles (i.e., with diameters smaller than 100 nm) may lead to long-  
57 term respiratory illness.<sup>22</sup> Consequently, it is important to ensure that secondary air injection  
58 designs achieve emission reductions throughout the particle size range.

59 Achieving comprehensive emission reductions using secondary air injection requires  
60 many design parameters to be optimized. For example, the airflow rate should be set at an  
61 optimal value that promotes effective turbulent mixing, but does not lower combustion zone  
62 temperatures excessively. Several publications demonstrate the importance of secondary air  
63 injection optimization in combustion appliances that utilize pelletized biomass fuels.<sup>12,13,18,19,23</sup>  
64 However, over 2 billion people do not have access to processed fuels, and must instead rely on  
65 unprocessed biomass, such as wood and dung.<sup>24</sup> Despite the potential benefits of air injection,

66 systematic studies of this technology in cookstoves that use unprocessed biomass fuels are not  
67 readily available.

68 In this paper, we present an experimental biomass cookstove platform and parametric  
69 testing approach to identify and optimize critical secondary air injection parameters that reduce  
70 CO, PM, and black carbon (BC) emissions from unprocessed wood combustion. We conducted  
71 over 130 experimental trials, systematically varying several air injection design parameters (e.g.,  
72 flow rate, velocity, position) to evaluate their effect on cooking performance and emissions.  
73 Size-resolved measurements of particle emissions were analyzed as a function of parametric  
74 cookstove settings to provide insight on the effects of secondary air injection on particle  
75 formation mechanisms, and inform future improved biomass cookstove designs.

## 76 **MATERIALS AND METHODS**

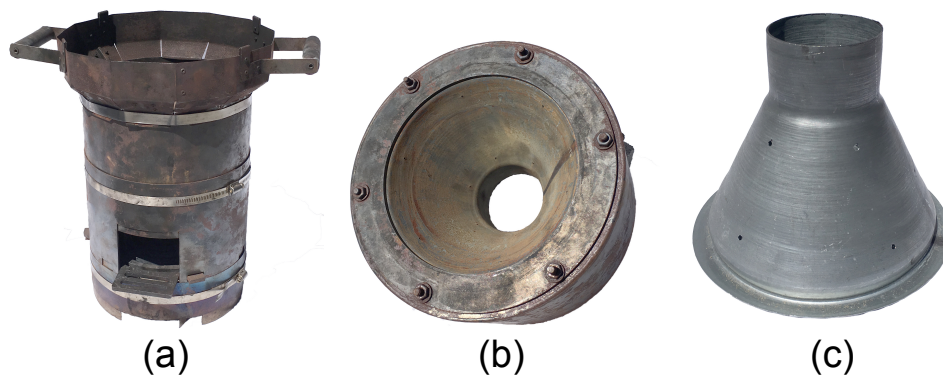
77 **Modular Air Injection Cookstove Design (MOD).** The MOD stove, shown in Figure 1,  
78 is a continuously fed, wood-burning cookstove designed to enable rapid adjustments of critical  
79 air injection design features. The MOD stove's general architecture is based on the Berkeley-  
80 Darfur Stove (BDS), using the same firebox design and accommodating the same cast-aluminum  
81 Darfuri cooking pot.<sup>6,21</sup> The MOD stove has a cylindrical firebox that is 178 mm (7 inch) in  
82 diameter with a front-facing fuel feed, and a cast-iron fuel grate. Above the firebox, there is a  
83 conical chimney (see Figure 1(c)) that reduces to a cylindrical extension, or 'throat', 76 mm (3  
84 inch) in diameter. The pot is supported above the throat, and surrounded by a skirt to increase  
85 heat transfer efficiency.

86 Primary air enters the firebox through the open fuel feed and adjustable openings in the  
87 stove body located below the fuel grate. Secondary air from a compressed air cylinder flows into  
88 a manifold inside the stove and is injected into the firebox through holes in the conical chimney,

89 as shown in Figure 2. The conical chimney is a removable pipe reducer known as a ‘cone’. These  
90 removable cones (one of which is shown in Figure 1(c)) allow for various air injection designs to  
91 be implemented and tested rapidly. New air injection patterns are created by drilling holes into a  
92 new cone, and mounted inside the manifold.

93 The MOD stove also incorporates design features to adjust the following parameters: (1)  
94 Primary air intake: the size of the opening in the stove body for primary air entrainment can be  
95 adjusted using a sliding ring, (2) Grate height: the fuel grate can be moved up and down,  
96 adjusting the distance between the fuel bed and the air injection holes in the conical manifold,  
97 and (3) Pot height: the pot sits on three bolts to adjust the height of the pot above the throat.  
98 Using these design features, shown in Figures S1 to S3, rapid, repeatable, and consistent  
99 parametric experiments can be conducted. However, the stove’s complex modular design and  
100 reliance on a compressed air cylinder make it uneconomical and impractical for field use.  
101 Instead, the lessons learned and design principles extracted from testing of the MOD stove are  
102 intended to inform future clean biomass cookstove designs for mass production and distribution.

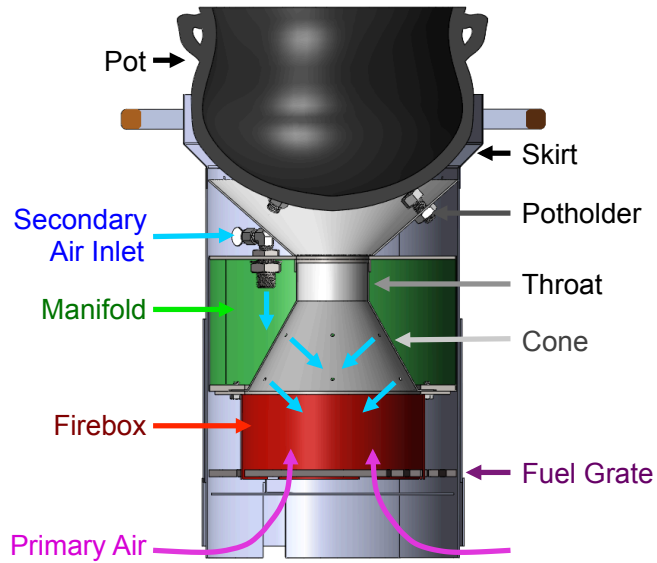
103



104

105

**Figure 1.** (a) MOD stove (b) Air injection manifold (c) Air injection cone



106

107

**Figure 2.** Cut view of MOD stove

108

109

110

111

112

113

114

115

116

117

118

119

120

121

**Experimental Set Up.** All experiments were conducted at the cookstove testing facility at Lawrence Berkeley National Laboratory (LBNL), schematically represented in Figure S4. Cookstoves are tested under a steel exhaust hood that completely captures pollutant emissions. Electric blowers exhaust emissions outside the building using a steel duct system. The flow rate through the duct is calculated using differential pressure measurements across a calibrated iris damper, and set to 5660 LPM (200 CFM) throughout testing to ensure replicability of measurements.

Particulate and gaseous emission concentrations in the duct are measured every second (1 Hz) using a suite of real-time instruments. Carbon monoxide (CO) and carbon dioxide (CO<sub>2</sub>) volume concentrations are measured using a California Analytical Instruments 600 Series gas analyzer. Real-time PM instruments sample emissions from the duct isokinetically using a secondary diluter (see Appendix III of the SI). Particle number concentrations are measured as a function of particle diameter from 5 nm to 2.5 μm using a TSI 3091 Fast Mobility Particle Sizer (FMPS), and a TSI 3321 Aerodynamic Particle Sizer (APS). BC mass concentrations are

122 measured using a Magee Scientific AE-22 Aethalometer. The total mass of PM with  
123 aerodynamic diameter  $\leq 2.5 \mu\text{m}$  ( $\text{PM}_{2.5}$ ) emitted during each cookstove experiment is measured  
124 gravimetrically using 47-mm filters. The gravimetric filter system samples PM emissions from  
125 the duct isokinetically using a dedicated probe. Detailed overviews of the experimental set-up  
126 and gravimetric  $\text{PM}_{2.5}$  measurement procedures are provided in section S-1.2 of the SI.

127 **Stove Testing Procedure.** Cookstove performance and emissions were measured during  
128 the high power, cold start phase of the Water Boiling Test (WBT) 4.2.3.<sup>25</sup> During this test phase,  
129 a fire is lit inside a stove that is initially at ambient temperature ('cold'), and operated at a high  
130 firepower to boil 5 L of water. The test ends when a full rolling boil is reached at a measured  
131 water temperature of  $99^\circ\text{C}$  (the nominal local boiling point). Pollutant emissions are typically  
132 more elevated during this phase of stove use because: (1) the cold stove and pot of water quench  
133 flames and absorb heat, thereby lowering combustion temperatures, (2) the cold fuel bed  
134 combusts poorly during initial lighting, and (3) the mass of harmful emissions released per  
135 energy delivered to the pot of water typically increases with firepower.<sup>6</sup> In this way, the cold  
136 start phase represents a 'worst-case' emissions scenario, and the design principles derived can be  
137 applied to other phases of stove use that are more forgiving to performance (e.g., hot start or  
138 simmer).

139 For each experiment, the stove was fueled with Douglas Fir wood cut into uniform pieces  
140 and dried to 7-9% moisture content on a wet basis. All tests were conducted at a constant high  
141 firepower setting of 5 kW to enable the immediate comparison of stove configurations.<sup>21</sup> A  
142 compressed air cylinder provided secondary air for the MOD stove using a two-stage regulator.  
143 The volumetric flow rate of secondary air was measured using a rotameter and adjusted using a  
144 valve. During preliminary trials, we observed that turning on the secondary air injection too soon

145 after ignition caused the fire to smolder or go out entirely. Consequently, air injection was  
146 initiated about 2 minutes after fuel ignition to ensure the fire was well established, thereby  
147 preventing quenching and extinction.

148 **Parametric Testing Procedure.** Five MOD stove design parameters were identified for  
149 experimental optimization: (1) Pot height, (2) Grate height, (3) Primary air intake size, (4)  
150 Secondary air injection pattern (number and arrangement of holes), and (5) Secondary air flow  
151 rate. Since testing results from solid biomass stoves are highly variable, replicate tests are  
152 required to accurately determine performance and emission levels at any given parametric stove  
153 configuration. In order to reduce the total testing time required to optimize the stove, exploratory  
154 trials were conducted using a simplified cold start procedure (see SI section S-1.4).

155 During exploratory testing, stove design parameters were methodically adjusted to reduce  
156 pollutant emissions while maintaining high thermal efficiency. Using data from 71 exploratory  
157 trials, optimal settings were identified for the following air injection design parameters: The gap  
158 between the pot and skirt is set to 15 mm (0.60 inch), the grate height is set to 57 mm (2.25 inch)  
159 below the air injection manifold, and the primary air intake is set to roughly 70% of the fully  
160 open position (an opening with an area of 4800 mm<sup>2</sup> (7.4 inch<sup>2161 efficient air injection patterns were identified for further parametric testing (shown in Figure S6).  
162 All exploratory testing results are provided in the SI.</sup>

163 Following exploratory testing, the two optimal air injection patterns were tested at flow  
164 rates of 21, 28, and 35 LPM (0.75, 1, and 1.25 CFM), for a total of six parametric configurations;  
165 all other parameters were maintained at the optimal values identified during exploratory testing.  
166 For each parametric configuration, 6 to 7 replicate tests were conducted. By adjusting the stove  
167 parameters in evenly distributed increments, parametric curves were generated to illuminate how

168 secondary air injection influences the stove's emissions and performance. Results from these  
169 initial 39 trials suggest that an air injection flow rate of 28 LPM is most effective, and so an  
170 additional 12 trials were conducted at this flow rate using both air injection patterns. These two  
171 final sets of 12 replicate tests enable the identification and validation of the optimal parametric  
172 stove configuration with a higher degree of confidence.

173 **Data Analysis and Metrics.** All stove performance and emissions metrics were  
174 calculated in accordance with the methods presented in section S-1.6 of the SI. Emission factors  
175 are normalized by the average thermal power delivered to the pot, known as cooking power, in  
176 units of kW-delivered (kWd). Cooking power is defined as the product of firepower and thermal  
177 efficiency, and represents the useful thermal power output of the cookstove. All data are  
178 presented with 90% confidence intervals calculated using Student's t-distribution.<sup>26,27</sup>

179 The MOD stove's performance and emissions are compared to those of a TSF using cold  
180 start testing data collected by Rapp et al. (2016) at the LBNL cookstove facility. The TSF was  
181 also tested at a firepower of 5 kW, with the same pot, fuel, experimental procedures, and  
182 instruments as used for the MOD stove testing.<sup>21</sup>

## 183 **RESULTS AND DISCUSSION**

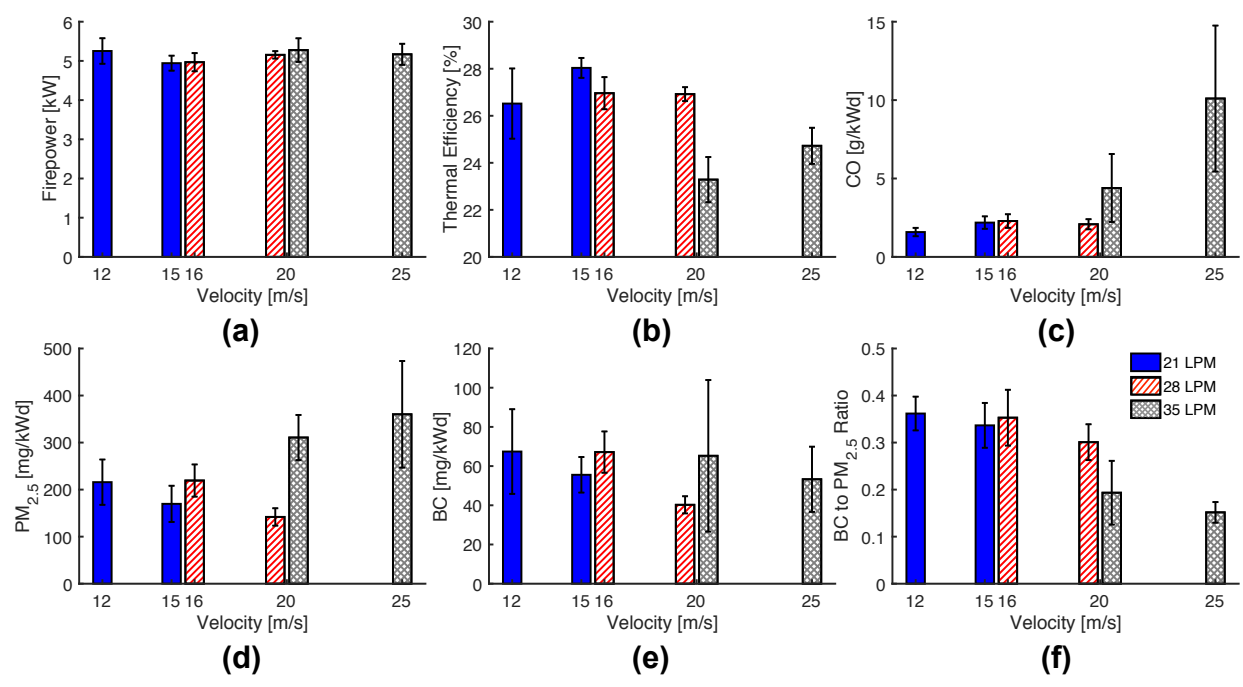
184 **Parametric Performance Metrics.** A total of 63 WBT cold start tests were conducted to  
185 identify the cleanest, most efficient combination of secondary air injection pattern and flow rate.  
186 The thermal efficiency and emissions of six MOD stove configurations are evaluated as a  
187 function of air injection flow rate and velocity, as shown in Figure 3. The air injection velocity is  
188 calculated using the air injection flow rate and total area of the holes in the air injection pattern,  
189 as outlined in section S-1.6 of the SI. Emission factors represent the total mass of pollutant  
190 emitted during the cold start test, normalized by the cooking power.

191 Firepower, shown in Figure 3(a), was maintained at  $5.1 \pm 0.1$  kW throughout parametric  
192 testing to provide consistency between experiments. Figure 3(b) shows that thermal efficiency  
193 remains around 27% for flow rates of 21 and 28 LPM, and decreases to about 24% at 35 LPM.  
194 The decrease in thermal efficiency at 35 LPM is likely caused by the abundance of injected air  
195 cooling the combustion zone, thereby reducing the stove's exhaust temperature even as  
196 firepower is held constant. The drop in exhaust temperature reduces the rate of heat transfer to  
197 the pot, and degrades the thermal performance of the stove.

198 Increasing CO emissions, shown in Figure 3(c), also suggest that air injection at 35 LPM  
199 is quenching the flame and cooling the combustion zone.<sup>18,28</sup> CO emissions from biomass  
200 combustion increase dramatically when combustion temperatures drop below  $\sim 800^\circ\text{C}$ , but  
201 remain relatively constant above this critical oxidation temperature.<sup>15,20</sup> Correspondingly, Figure  
202 3(c) shows that CO emissions are relatively constant as air injection increases from 21 to 28  
203 LPM, but more than double when flow rate increases from 28 to 35 LPM. Additionally, as air  
204 injection velocity increases from 20 to 25 m/s at 35 LPM, the magnitude and variability of CO  
205 emissions both increase substantially, suggesting that enhanced turbulent mixing of excess  
206 secondary air is quenching the flame.

207  $\text{PM}_{2.5}$  emissions follow the same trend as CO emissions: When the flow rate is increased  
208 from 28 to 35 LPM at a constant velocity of 20 m/s,  $\text{PM}_{2.5}$  emissions nearly double, and continue  
209 to rise as air injection velocity increases at 35 LPM (see Figure 3(d)). PM formation and growth  
210 occur when volatile gases in the exhaust cool and nucleate into solid particles or condense onto  
211 existing particles.<sup>29</sup> Similarly to CO, many volatile organic compounds that form PM, such as  
212 polycyclic aromatic hydrocarbons (PAH), oxidize around  $750\text{-}800^\circ\text{C}$ . At a flow rate of 35 LPM,  
213 excessive secondary air injection likely lowers the combustion zone temperature below this

214 critical oxidation point, thereby enhancing particle nucleation and condensation.<sup>20</sup> Earlier studies  
 215 have also shown that high CO emissions are usually accompanied by higher emissions of volatile  
 216 organic compounds and other carbonaceous species that contribute to PM<sub>2.5</sub> mass emissions.<sup>20,28</sup>



217  
 218 **Figure 3.** Cold start performance and emissions of the MOD stove as a function of secondary air  
 219 injection flow rate (represented by bar color) and velocity (shown on the horizontal axis): (a)  
 220 Firepower (kW); (b) Thermal efficiency (%), (c) Carbon monoxide (CO) emissions (g/kWd), (d)  
 221 Particulate matter (PM<sub>2.5</sub>) emissions (mg/kWd), (e) Black carbon (BC) emissions (mg/kWd), (f)  
 222 BC to PM<sub>2.5</sub> ratio. Bar heights represent the metric mean at each stove configuration, and error  
 223 bars represent the corresponding 90% confidence interval. Emissions are reported as the total  
 224 mass of pollutant emitted during the cold start test normalized by the cooking power.

225 PM<sub>2.5</sub> composition can also provide insight into combustion conditions. PM<sub>2.5</sub> emissions  
 226 from biomass combustion contain both inorganic particles, such as salt compounds and heavy  
 227 metals, and organic particles consisting of either BC or tars.<sup>30</sup> The effect of air injection flow rate

228 and velocity on BC emissions – optically absorbing soot that forms directly in the flame – is  
229 shown in Figure 3(e). At each flow rate setting, BC emissions decrease with increasing air  
230 injection velocity, as additional oxygen and turbulent mixing help to eliminate fuel-rich zones  
231 where BC is formed.<sup>31</sup> However, BC emissions at the low velocity setting for each air injection  
232 flow rate remain nearly constant (~70 mg/kWd). As flow rate increases, combustion zone  
233 temperatures are lowered, and the rate of BC oxidation decreases.<sup>32,33</sup> For these combustion  
234 conditions, the resulting increase in BC emissions effectively negates the reductions incurred  
235 from increasing turbulent mixing.<sup>15,34</sup>

236 Unlike CO and PM<sub>2.5</sub>, BC emissions at a secondary air flow rate of 35 LPM generally  
237 decrease when injection velocity increases from 20 to 25 m/s, suggesting that combustion zone  
238 temperatures are sufficiently elevated to oxidize BC. BC from biomass combustion has been  
239 shown to oxidize around 350 °C.<sup>34,35</sup> This oxidation temperature is much lower than that of CO  
240 and many of the volatile compounds that form PM<sub>2.5</sub> (around 750 - 800 °C), and enables BC  
241 reductions throughout the parametric range.

242 In order to better understand the effect of secondary air injection on PM<sub>2.5</sub> composition,  
243 the ratio of BC to PM<sub>2.5</sub> emissions is shown in Figure 3(f). The figure shows that the BC to PM<sub>2.5</sub>  
244 ratio is stable at air injection flow rates of 21 and 28 LPM, but decreases sharply at 35 LPM.  
245 This trend further illustrates that BC is effectively oxidized throughout the parametric range, but  
246 excessive cooling at a flow rate of 35 LPM quenches the flame and increases overall PM<sub>2.5</sub> mass  
247 emissions. Furthermore, the BC to PM<sub>2.5</sub> ratio at each flow rate setting remains relatively  
248 constant as air injection velocity increases, suggesting that PM<sub>2.5</sub> composition is more dependent  
249 on combustion temperature than turbulent mixing.

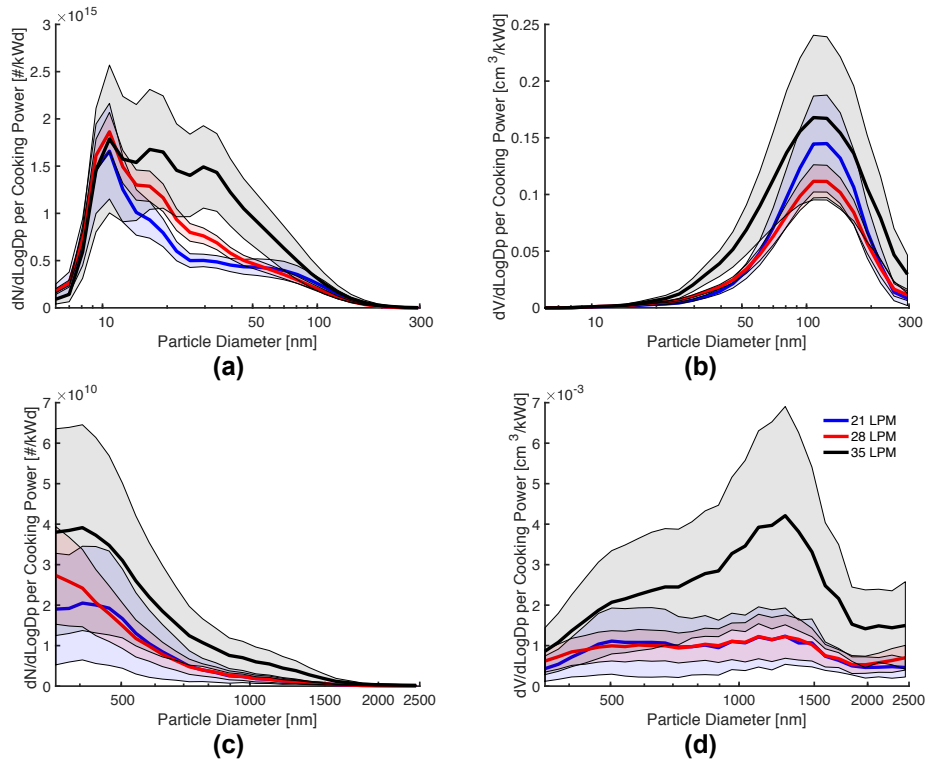
250 Overall, the metrics in Figure 3 indicate that a flow rate of 28 LPM at an air injection  
251 velocity of 20 m/s is the optimal configuration for this stove. In this configuration, the stove  
252 minimizes emissions of pollutants, while maintaining high thermal efficiency. Although thermal  
253 efficiency and CO emissions improve slightly at a flow rate 21 LPM, the metrics show that 28  
254 LPM at 20 m/s provides an optimal balance between maintaining high thermal performance and  
255 lowering pollutant emissions. Compared to a TSF, the optimal configuration of the MOD stove  
256 uniformly reduces CO, PM<sub>2.5</sub>, and BC emissions by about 90%, while increasing thermal  
257 efficiency from 23.3 ± 0.7% to 26.4 ± 0.4% (see section S-2.3 of the SI).

258 **Size-Resolved Particle Emissions with Varying Air Injection Flow Rate.** The optimal  
259 injection pattern identified in Figure 3 (Cone 1, shown in Figure S6) was tested at 21, 28, and 35  
260 LPM (corresponding to air injection velocities of 15, 20, and 25 m/s, respectively). Figure 4  
261 shows the mean particle distribution of replicate trials conducted at each air injection flow rate,  
262 with shaded areas representing 90% confidence intervals of the set. Each distribution represents  
263 the total particle number and volume emitted over the cold start, normalized by the cooking  
264 power. FMPS measurements span from 6 to 295 nm, while APS measurements span from 351 to  
265 2500 nm. The last four bins of the FMPS measurement span (from 341 to 524 nm) are omitted,  
266 and the APS measurements have been converted from aerodynamic to electrical mobility particle  
267 diameter (see section S-1.7 of the SI).<sup>36</sup>

268 Figure 4(a) reveals that the number distribution at each secondary air injection flow rate  
269 setting has a maximum peak at a particle diameter of around 10 nm, representing primary  
270 particles formed by the nucleation of volatile gases in the exhaust or soot generation in the  
271 flame.<sup>37-39</sup> Furthermore, the figure illustrates that as flow rate increases, the number of particles  
272 from 10 to 50 nm also increases. These results suggest that combustion zone temperatures

273 decrease with increasing flow rate, thereby inhibiting the oxidation of volatile organic gases and  
274 other PM-forming species.<sup>15</sup> The increased emission of volatile gases and lower combustion  
275 zone temperatures both promote more PM nucleation.<sup>20,28</sup> The number distribution at flow rate of  
276 35 LPM has two prominent peaks at particle diameters of around 20 and 30 nm that diminish as  
277 flow rate decreases. These two peaks likely represent primary particle species that begin to form  
278 as combustion zone temperatures decrease at higher air injection flow rates.<sup>31,39</sup>

279 The particle volume distributions in Figure 4(b) show a unimodal peak centered at a  
280 particle diameter of around 100 nm, closely mirroring particle distribution measurements from  
281 other biomass combustion studies.<sup>15,28,38,40</sup> The figure also shows that a secondary air injection  
282 flow rate of 28 LPM yields the lowest volume distribution, indicating that this provides sufficient  
283 turbulent mixing to promote better fuel oxidation without lowering combustion zone  
284 temperatures excessively. The increased particle volume generation at both 21 LPM and 35 LPM  
285 suggests that 21 LPM does not provide enough turbulent mixing while 35 LPM cools the  
286 combustion zone.

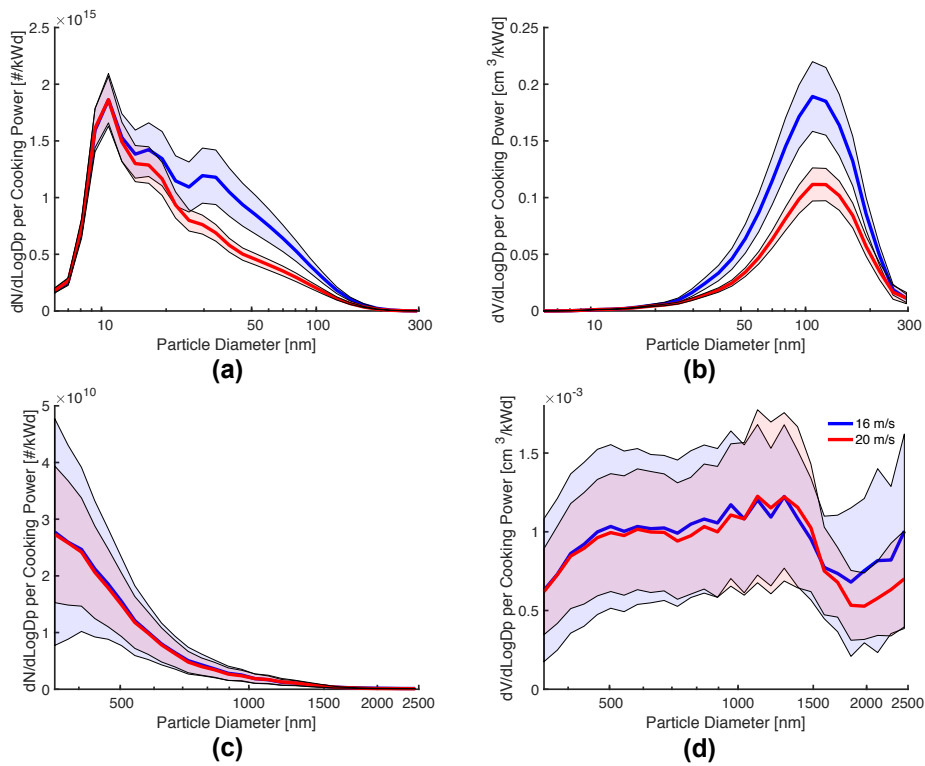


287

288 **Figure 4.** Size-resolved distribution of total particle number or volume emitted during the cold  
 289 start, normalized by the average cooking power, for three air injection flow rate settings: (a)  
 290 FMPS particle number distribution, (b) FMPS particle volume distribution, (c) APS particle  
 291 number distribution, (d) APS particle volume distribution

292 Figure 4(c) and 4(d) show that the number and volume distributions of particles larger  
 293 than 350 nm (up to 2500 nm) are roughly similar for flow rates of 21 and 28 LPM, but increase  
 294 appreciably at 35 LPM, further indicating that combustion zone temperatures drop below the  
 295 critical oxidation temperature of certain PM forming species.<sup>28</sup> The distinct peak in the volume  
 296 distribution at 1280 nm (see Figure 4(d)) is the result of primary particle growth through  
 297 condensation and agglomeration, promoted by the low combustion temperatures and high  
 298 turbulent mixing at a flow rate of 35 LPM.<sup>38,39</sup>

299 **Size-Resolved Particle Emissions with Varying Air Injection Velocity.** Air injection  
 300 flow rate was maintained at the optimal 28 LPM setting, while velocity was varied using the two  
 301 different air injection patterns. Figure 5 provides the resulting particle number and volume  
 302 distributions at secondary air injection velocities of 16 and 20 m/s. For both air injection  
 303 velocities, the peaks in the particle number distributions at a diameter of 10 nm are nearly  
 304 identical (see Figure 5(a)). However, increasing air injection velocity reduces particle number  
 305 emissions above 30 nm. Additionally, the peaks at particle diameters of 20 nm and 30 nm  
 306 become less distinguishable as air injection velocity increases from 16 m/s to 20 m/s. These  
 307 results indicate that additional turbulent mixing at higher air injection velocity promotes more  
 308 oxidation of volatile gases, and reduces the formation of primary particles and subsequent  
 309 particle growth through condensation.<sup>15,28</sup> Correspondingly, Figure 5(b) shows that increasing air  
 310 injection velocity reduces the particle volume distribution by almost 50%.



312 **Figure 5.** Size-resolved distribution of total particle number or volume emitted during the cold  
313 start, normalized by the average cooking power, for two air injection velocity settings at a flow  
314 rate of 28 LPM: (a) FMPS particle number distribution, (b) FMPS particle volume distribution,  
315 (c) APS particle number distribution, (d) APS particle volume distribution

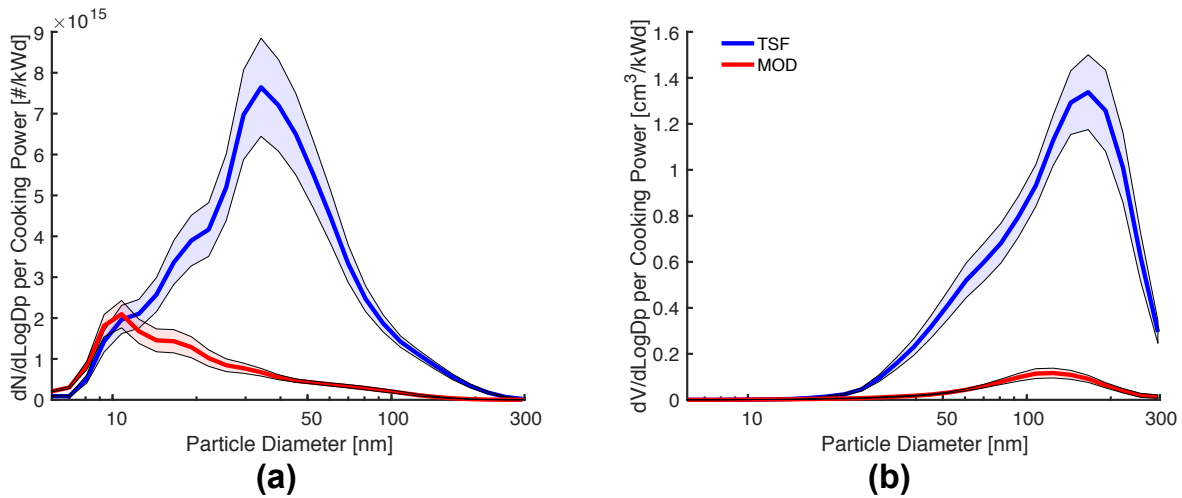
316 For particles larger than 350 nm (up to 2500 nm), the particle number and volume  
317 distributions at both air injection velocities are nearly identical (see Figure 5(c) and 5(d)). These  
318 results indicate that air injection at 28 LPM promotes more complete fuel oxidation and reduces  
319 particle growth above 350 nm, independently of air injection velocity. However, for a flow rate  
320 of 21 LPM, the number of particles larger than 350 nm increases significantly as air injection  
321 velocity decreases, suggesting that a lack of turbulent mixing can promote particle growth under  
322 certain conditions (see Figure S9). Particle number and volume distributions for the air injection  
323 velocities tested at 21 LPM and 35 LPM are provided in section S-2.4 of the SI.

324 **Size-Resolved Particle Emissions compared to Three-Stone Fire.** Figure 4 and 5 show  
325 that the MOD stove provides the greatest particle emission reductions at a secondary air injection  
326 flow rate of 28 LPM and injection velocity of 20 m/s (which agrees with the gravimetric  $PM_{2.5}$   
327 measurements provided in Figure 3(d)). However, it should also be noted that the emission of  
328 particles smaller than 50 nm in diameter are somewhat lower for an air injection flow rate of 21  
329 LPM, highlighting the importance of maintaining high combustion zone temperatures to  
330 minimize ultrafine particle emissions.

331 Figure 6 compares FMPS particle number and volume distributions of the optimal MOD  
332 stove configuration (28 LPM and 20 m/s) to the TSF. Figure 6(a) shows that the MOD stove  
333 reduces the total number of ultrafine particles (with a diameter less than 100 nm) by about 75%  
334 relative to the TSF. However, for particles less than 10 nm in diameter, the MOD stove generates

335 roughly the same number of particles as the TSF. Given the MOD stove's improved combustion  
336 conditions (as demonstrated by the significant emissions reductions), it is possible that these 10  
337 nm particles nucleate from inorganic volatile gases, such as salts. These inorganic compounds  
338 volatilize more readily at higher fuel bed temperatures, and result in particle emissions that  
339 cannot be reduced through improvements in the combustion process.<sup>12,14,30,40</sup>

340 Figure 6(b) shows that volumetric particle emissions are reduced by an order of  
341 magnitude throughout the diameter range provided, which agrees with the gravimetric particle  
342 measurements provided in Table S2. For particles larger than 350 nm in diameter, the MOD  
343 stove uniformly reduces particle number and volume generation by nearly two orders of  
344 magnitude. Number and volume distributions for particles larger than 350 nm can be found in  
345 section S-2.5 of the SI.



346

347 **Figure 6.** Size-resolved distribution of total particle number or volume emitted during the cold  
348 start, normalized by the average cooking power for a three-stone fire (TSF) and the MOD stove  
349 operating at an air injection flow rate of 28 LPM and velocity of 20 m/s: (a) FMPS particle  
350 number distribution, (b) FMPS particle volume distribution

351 Using the experimentally optimized configuration, the MOD stove reduces CO, PM<sub>2.5</sub>,  
352 and BC mass emissions by about 90%, and reduces ultrafine particle number emissions by about  
353 75%, compared to a TSF. The results also demonstrate that pollutant emissions are highly  
354 sensitive to secondary air injection design parameters, such as flow rate and velocity. Therefore,  
355 improved cookstove designs that implement air injection should be experimentally optimized  
356 and validated to ensure that pollutant mass emissions are minimized, and particle emissions are  
357 reduced across the full range of PM diameters. While this study focuses on modulating five stove  
358 design parameters to reduce emissions, it is also important to investigate other operational  
359 factors, such as firepower, fuel condition (moisture content, size, surface area), and secondary air  
360 temperature. Furthermore, future studies should incorporate additional instrumentation to enable  
361 deeper investigation of the combustion process, such as thermocouples to measure combustion  
362 temperatures, and/or a thermal-optical analyzer to examine the composition of PM emitted.

363 Overall, this study demonstrates that experimental optimization enables the design of  
364 wood-burning stoves that both reduce pollutant emissions and improve cooking performance.  
365 The experimental approach and results presented can inform the development of air injection  
366 stoves that reduce harmful smoke exposure in the one billion households currently relying on  
367 biomass cooking fuels.

368 **SUPPORTING INFORMATION**

369 Additional information on the Modular stove design, experimental setup, and results are  
370 available in the Supporting Information. This material is available free of charge via the Internet  
371 at <http://pubs.acs.org/>.

372 **ACKNOWLEDGMENT**

373 This work was performed at the Lawrence Berkeley National Laboratory, operated by the  
374 University of California, under DOE Contract DE-AC02-05CH11231. We gratefully  
375 acknowledge support for this work from DOE's Biomass Energy Technologies Office. Author  
376 Julien J. Caubel is grateful for support from the National Science Foundation's Graduate  
377 Research Fellowship Program.

378 The authors acknowledge Brahim Idrissi Kaitouni, Allen Boltz, and Arjun Kaul for their  
379 countless hours in the laboratory testing the cookstoves and collecting data. We would also like  
380 to thank Dr. Thomas Kirchstetter for guidance in post-processing the particle emissions data and  
381 Gary Hubbard for developing the software tools to simplify data collection from all of our  
382 instruments.

383 **ABBREVIATIONS**

384 APS, Aerodynamic Particle Sizer; BC, Black Carbon; BDS, Berkeley-Darfur Stove; CAI,  
385 California Analytical Instruments; CO<sub>2</sub>, Carbon Dioxide; CO, Carbon Monoxide; EC, Elemental  
386 Carbon; FMPS, Fast Mobility Particle Sizer; kWd, kilowatt of power delivered to the pot;  
387 LBNL, Lawrence Berkeley National Laboratory; MOD, Modular Stove; PAH, Polycyclic  
388 Aromatic Hydrocarbon; PM, Particulate Matter; PM<sub>2.5</sub>, Particulate Matter with an aerodynamic  
389 diameter  $\leq 2.5 \mu\text{m}$ ; ppm, parts per million; TSF, Three Stone Fire; WBT, Water Boiling Test.

390 **REFERENCES**

- 391 (1) Bonjour, S.; Adair-Rohani, H.; Wolf, J.; Bruce, N. G.; Mehta, S.; Prüss-Ustün, A.;  
392 Lahiff, M.; Rehfuess, E. A.; Mishra, V.; Smith, K. R. Solid Fuel Use for Household  
393 Cooking: Country and Regional Estimates for 1980–2010. *Environ. Health Perspect.*  
394 **2013**, *121* (7), 784–790.
- 395 (2) Bruce, N. G.; Perez-Padilla, R.; Albalak, R. Indoor air pollution in developing countries:  
396 a major environmental and public health challenge. *Bulletin of the World Health*  
397 *Organization* **2000**, *78* (9), 1078–1092.
- 398 (3) Lim, S. S.; Vos, T.; Flaxman, A. D.; Danaei, G.; Shibuya, K.; Adair-Rohani, H.;  
399 AlMazroa, M. A.; Amann, M.; Anderson, R. H.; Andrews, K. G.; et al. A comparative  
400 risk assessment of burden of disease and injury attributable to 67 risk factors and risk  
401 factor clusters in 21 regions, 1990–2010: a systematic analysis for the Global Burden of  
402 Disease Study 2010. *The Lancet* **2012**, *380* (9859), 2224–2260.
- 403 (4) Legros, G.; Havet, I.; Bruce, N. G.; Bonjour, S. *The Energy Access Situation in*  
404 *Developing Countries*; United Nations Development Programme (UNDP): New York,  
405 2009; pp 1–142.
- 406 (5) Birol, F.; Argiri, M.; Cozzi, L.; Dowling, P.; Emoto, H.; Lyons, L.; Malyshev, T. *World*  
407 *Energy Outlook 2006*; Priddle, R., Ed.; International Energy Agency, 2006; pp 1–601.
- 408 (6) Jetter, J.; Zhao, Y.; Smith, K. R.; Khan, B.; Yelverton, T.; DeCarlo, P.; Hays, M. D.  
409 Pollutant Emissions and Energy Efficiency under Controlled Conditions for Household  
410 Biomass Cookstoves and Implications for Metrics Useful in Setting International Test  
411 Standards. *Environ. Sci. Technol.* **2012**, *46* (19), 10827–10834.
- 412 (7) *WHO Air quality guidelines for particulate matter, ozone, nitrogen dioxide and sulfur*  
413 *dioxide*; World Health Organization, 2005.

- 414 (8) Smith, K. R.; Dutta, K.; Chengappa, C.; Gusain, P. P. S.; Berrueta, O. M. A. V.;  
415 Edwards, R.; Bailis, R.; Shields, K. N. Monitoring and evaluation of improved biomass  
416 cookstove programs for indoor air quality and stove performance: conclusions from the  
417 Household Energy and Health Project. *Energy for Sustainable Development* **2007**, *11*  
418 (2), 5–18.
- 419 (9) Chen, C.; Zeger, S.; Breysse, P.; Katz, J.; Checkley, W.; Curriero, F. C.; Tielsch, J. M.  
420 Estimating Indoor PM<sub>2.5</sub> and CO Concentrations in Households in Southern Nepal: The  
421 Nepal Cookstove Intervention Trials. *PLoS ONE* **2016**, *11* (7), e0157984–17.
- 422 (10) Nussbaumer, T. Combustion and Co-combustion of Biomass: Fundamentals,  
423 Technologies, and Primary Measures for Emission Reduction †. *Energy Fuels* **2003**, *17*  
424 (6), 1510–1521.
- 425 (11) Edwards, R.; Karnani, S.; Fisher, E. M.; Johnson, M.; Naeher, L.; Smith, K. R.;  
426 Morawska, L. *WHO Indoor Air Quality Guidelines: Household fuel Combustion*; World  
427 Health Organization, 2014; pp 1–42.
- 428 (12) Lamberg, H.; Sippula, O.; Tissari, J.; Jokiniemi, J. Effects of Air Staging and Load on  
429 Fine-Particle and Gaseous Emissions from a Small-Scale Pellet Boiler. *Energy Fuels*  
430 **2011**, *25* (11), 4952–4960.
- 431 (13) Lyngfelt, A.; Leckner, B. Combustion of wood-chips in circulating fluidized bed boilers  
432 — NO and CO emissions as functions of temperature and air-staging. *Fuel* **1999**, No. 78,  
433 1065–1072.
- 434 (14) Carroll, J. P.; Finnan, J. M.; Biedermann, F.; Brunner, T.; Obernberger, I. Air staging to  
435 reduce emissions from energy crop combustion in small scale applications. *Fuel* **2015**,  
436 *155*, 37–43.

- 437 (15) Nuutinen, K.; Jokiniemi, J.; Sippula, O.; Lamberg, H.; Sutinen, J.; Horttanainen, P.;  
438 Tissari, J. Effect of air staging on fine particle, dust and gaseous emissions from  
439 masonry heaters. *Biomass and Bioenergy* **2014**, *67*, 167–178.
- 440 (16) Sutar, K. B.; Kohli, S.; Ravi, M. R.; Ray, A. Biomass cookstoves: A review of technical  
441 aspects. *Renewable and Sustainable Energy Reviews* **2015**, *41*, 1128–1166.
- 442 (17) Still, D.; Bentson, S.; Li, H. Results of Laboratory Testing of 15 Cookstove Designs in  
443 Accordance with the ISO/IWA Tiers of Performance. *EcoHealth* **2015**, *12*, 12–24.
- 444 (18) Okasha, F. Staged combustion of rice straw in a fluidized bed. *Experimental Thermal  
445 and Fluid Science* **2007**, *32* (1), 52–59.
- 446 (19) Tryner, J.; Tillotson, J. W.; Baumgardner, M. E.; Mohr, J. T.; DeFoort, M. W.;  
447 Marchese, A. J. The Effects of Air Flow Rates, Secondary Air Inlet Geometry, Fuel  
448 Type, and Operating Mode on the Performance of Gasifier Cookstoves. *Environ. Sci.  
449 Technol.* **2016**, *50* (17), 9754–9763.
- 450 (20) Pettersson, E.; Lindmark, F.; Öhman, M.; Nordin, A.; Westerholm, R.; Boman, C.  
451 Design Changes in a Fixed-Bed Pellet Combustion Device: Effects of Temperature and  
452 Residence Time on Emission Performance. *Energy Fuels* **2010**, *24* (2), 1333–1340.
- 453 (21) Rapp, V. H.; Caubel, J. J.; Wilson, D. L.; Gadgil, A. J. Reducing Ultrafine Particle  
454 Emissions Using Air Injection in Wood-Burning Cookstoves. *Environ. Sci. Technol.*  
455 **2016**, *50* (15), 8368–8374.
- 456 (22) Valavanidis, A.; Fiotakis, K.; Vlachogianni, T. Airborne Particulate Matter and Human  
457 Health: Toxicological Assessment and Importance of Size and Composition of Particles  
458 for Oxidative Damage and Carcinogenic Mechanisms. *Journal of Environmental Science  
459 and Health, Part C* **2008**, *26* (4), 339–362.

- 460 (23) Wiinikka, H.; Gebart, R. Critical Parameters for Particle Emissions in Small-Scale  
461 Fixed-Bed Combustion of Wood Pellets. *Energy Fuels* **2004**, *18* (4), 897–907.
- 462 (24) Malla, S.; Timilsina, G. R. *Household Cooking Fuel Choice and Adoption of Improved*  
463 *Cookstoves in Developing Countries*; The World Bank, 2014; pp 1–52.
- 464 (25) *The Water Boiling Test*, 4 ed.; Global Alliance for Clean Cookstoves, 2014; pp 1–89.
- 465 (26) Taylor, J. R. *An introduction to error analysis: The study of uncertainties in physical*  
466 *measurements*; University Science Books: Sausalito, CA, 1997; pp 1–1.
- 467 (27) Wang, Y.; Sohn, M. D.; Wang, Y.; Lask, K. M.; Kirchstetter, T. W.; Gadgil, A. J. How  
468 many replicate tests are needed to test cookstove performance and emissions? — Three  
469 is not always adequate. *Energy for Sustainable Development* **2014**, *20*, 21–29.
- 470 (28) Johansson, L. S.; Leckner, B.; Gustavsson, L.; Cooper, D.; Tullin, C.; Potter, A.  
471 Emission characteristics of modern and old-type residential boilers fired with wood logs  
472 and wood pellets. *Atmospheric Environment* **2004**, *38* (25), 4183–4195.
- 473 (29) Torvela, T.; Tissari, J.; Sippula, O.; Kaivosoja, T.; Leskinen, J.; Virén, A.; Lähde, A.;  
474 Jokiniemi, J. Effect of wood combustion conditions on the morphology of freshly  
475 emitted fine particles. *Atmospheric Environment* **2014**, *87*, 65–76.
- 476 (30) Kelz, J.; Brunner, T.; Obernberger, I.; Jalava, P.; Hirvonen, M. R. PM emissions from  
477 old and modern biomass combustion systems and their health effects. **2010**.
- 478 (31) Obaidullah, M.; Bram, S.; Verma, V. K.; De Ruyck, J. A Review on Particle Emissions  
479 from Small Scale Biomass Combustion. *International Journal of Renewable Energy*  
480 *Research* **2012**, *2* (1), 1–13.
- 481 (32) Jiang, M.; Wu, Y.; Lin, G.; Xu, L.; Chen, Z.; Fu, F. Pyrolysis and thermal-oxidation  
482 characterization of organic carbon and black carbon aerosols. *Science of the Total*

- 483 *Environment, The* **2011**, 409 (20), 4449–4455.
- 484 (33) Brunner, T.; Barnthaler, G.; Obernberger, I. Evaluation of Parameters Determining PM  
485 Emissions and their Chemical Composition in Modern Residential Biomass Heating  
486 Appliances; 2008; pp 81–86.
- 487 (34) Petzold, A.; Ogren, J. A.; Fiebig, M.; Laj, P.; Li, S. M.; Baltensperger, U.; Holzer-Popp,  
488 T.; Kinne, S.; Pappalardo, G.; Sugimoto, N.; et al. Recommendations for reporting  
489 “black carbon” measurements. *Atmos. Chem. Phys.* **2013**, 13 (16), 8365–8379.
- 490 (35) Elmquist, M.; Cornelissen, G.; Kukulska, Z.; Gustafsson, Ö. Distinct oxidative stabilities  
491 of char versus soot black carbon: Implications for quantification and environmental  
492 recalcitrance. *Global Biogeochem. Cycles* **2006**, 20 (2), 1–11.
- 493 (36) Khlystov, A.; Stanier, C.; Pandis, S. N. An Algorithm for Combining Electrical Mobility  
494 and Aerodynamic Size Distributions Data when Measuring Ambient Aerosol. *Aerosol  
495 Science and Technology* **2004**, 38 (S1), 229–238.
- 496 (37) Just, B.; Rogak, S.; Kandlikar, M. Characterization of Ultrafine Particulate Matter from  
497 Traditional and Improved Biomass Cookstoves. *Environ. Sci. Technol.* **2013**, 47, 3506–  
498 3512.
- 499 (38) Jöller, M.; Brunner, T.; Obernberger, I. Modeling of aerosol formation during biomass  
500 combustion for various furnace and boiler types. *Fuel Processing Technology* **2007**, 88,  
501 1136–1147.
- 502 (39) Obernberger, I.; Brunner, T.; Barnthaler, G. Fine Particulate Emissions From Modern  
503 Austrian Small-Scale Biomass Combustion Plants; 2011; Vol. 15, pp 1–12.
- 504 (40) Wiinikka, H.; Gebart, R. The Influence of Air Distribution Rate on Particle Emissions in  
505 Fixed Bed Combustion of Biomass. *Combustion Science and Technology* **2005**, 177 (9),

506

1747-1766.

507